Second-order finite-element projection method for 3D flows

J.-L. Guermond[1] and L. Quartapelle[2]

[1] LIMSI–CNRS, BP 133, 91403 Orsay, France, (guermond@limsi.fr)
[2] Dipartimento di Fisica del Politecnico di Milano, Piazza L. da Vinci, 32 20133 Milano, Italy.

Key Words: INCOMPRESSIBLE NAVIER–STOKES EQUATIONS, INCREMENTAL PROJECTION METHOD, SECOND ORDER SCHEME, FINITE ELEMENTS

1 Introduction

Achieving high-order time accuracy in the solution of the incompressible Navier–Stokes equations by means of projection methods is a nontrivial task. In fact, a basic feature of projection methods is the uncoupling of the advection–diffusion mechanism from the incompressibility condition, the consequence of this uncoupling being the introduction of a *time-splitting error* that is an obstacle to develop high order schemes. In particular, the accuracy of the *non*incremental projection method introduced by Chorin (1969) and Temam (1968) is limited by an irreducible time-splitting error of $\mathcal{O}(\Delta t)$ Rannacher (1992) that makes second-order accuracy impossible. This limitation is not present in the *incremental* version of the projection method, also known as "pressure correction method", originally proposed by Goda (1979) in a finite difference context. The finite element counterpart of this scheme based on a first-order Euler time-discretization has been analyzed in Guermond (1994) and employed successfully in Guermond and Quartapelle (1997), where its time-splitting error has been numerically shown to be of $\mathcal{O}((\Delta t)^2)$. This result has been proved in Guermond (1997), where a new $(\Delta t)^2$-accurate projection scheme based on the three-level Backward Difference Formula has been proposed. The aim of this paper is to demonstrate the second-order accuracy of the incremental BDF method by means of numerical tests and to illustrate a finite element implementation of this scheme to simulate three dimensional realistic flows.

2 Incremental projection method

Consider the unsteady Navier-Stokes problem: Find the velocity $\boldsymbol{u}$ and the pressure p (up to a constant) so that, $\boldsymbol{u}_{|t=0} = \boldsymbol{u}_0$ and

$$\begin{cases} \frac{\partial \boldsymbol{u}}{\partial t} - \nu \nabla^2 \boldsymbol{u} + (\boldsymbol{u} \cdot \nabla)\boldsymbol{u} + \nabla p = \boldsymbol{f}, \\ \nabla \cdot \boldsymbol{u} = 0, \\ \boldsymbol{u}_{|\partial\Omega} = \boldsymbol{b}, \end{cases} \tag{2.1}$$

where ν is the viscosity, $\boldsymbol{f}$ is a known body force, $\boldsymbol{b}$ is the velocity prescribed on the boundary $\partial\Omega$, and $\boldsymbol{u}_0$ is the divergence-free initial velocity field. The

boundary and the data are assumed to be regular enough and to satisfy all the compatibility conditions needed for a smooth solution to exist for all time.

The incremental version of the fractional-step method consists in a time marching technique that makes explicit the pressure at the viscous step and corrects it at the projection step by evaluating a pressure increment to enforce the incompressibility condition. Setting $\boldsymbol{u}^0 = \boldsymbol{u}_0$ and assuming p^0 to be known, for $k \geq 0$ one has to solve: First, the advection–diffusion step

$$\begin{cases} \dfrac{\boldsymbol{u}^{k+1} - i^{\mathrm{t}}\,\widehat{\boldsymbol{u}}^{k}}{\Delta t} - \nu\nabla^2\boldsymbol{u}^{k+1} + (\boldsymbol{u}^k\cdot\nabla)\boldsymbol{u}^{k+1} + \frac{1}{2}(\nabla\cdot\boldsymbol{u}^k)\boldsymbol{u}^{k+1} = \boldsymbol{f}^{k+1} - \nabla p^k, \\ \boldsymbol{u}^{k+1}{}_{|\partial\Omega} = \boldsymbol{b}^{k+1}; \end{cases} \tag{2.2}$$

then, perform the projection step in the incremental form:

$$\begin{cases} \dfrac{\widehat{\boldsymbol{u}}^{k+1} - i\,\boldsymbol{u}^{k+1}}{\Delta t} + \widehat{\nabla}(p^{k+1} - p^k) = 0, \\ \widehat{\nabla}\cdot\widehat{\boldsymbol{u}}^{k+1} = 0, \qquad \boldsymbol{n}\cdot\widehat{\boldsymbol{u}}^{k+1}{}_{|\partial\Omega} = \boldsymbol{n}\cdot\boldsymbol{b}^{k+1}. \end{cases} \tag{2.3}$$

An important feature of this method is the difference, in terms of functional setting, that exists between the viscous step and the projection step, Guermond and Quartapelle (1998). The first half-step constitutes an elliptic boundary value problem for an intermediate velocity $\boldsymbol{u}^{k+1}$ accounting for viscosity and convection, whereas the second half-step represents an inviscid problem that determines the end-of-step divergence-free velocity field $\widehat{\boldsymbol{u}}^{k+1}$ together with a suitable approximation of the pressure increment $(p^{k+1} - p^k)$. As a consequence, boundary conditions of a different kind are imposed on the velocity fields that are calculated in the two half-steps. To emphasize the occurrence of two different vector spaces for the velocity, we use the notation $\boldsymbol{u}$ and $\widehat{\boldsymbol{u}}$. Similarly, the two operators $\nabla\cdot$ and $\widehat{\nabla}\cdot$ occurring in the two steps are distinguished since they act on vector fields belonging to spaces which are endowed with very different regularities, namely, $\boldsymbol{H}^1$ and $\boldsymbol{H}^{\mathrm{div}}$ (or possibly $\boldsymbol{L}^2$), respectively. We also introduce the injection operator $i : \boldsymbol{H}^1_0 \longrightarrow \boldsymbol{H}^{\mathrm{div}}_0$ and its transpose i^{t}. Indeed, $\widehat{\nabla}\cdot : \boldsymbol{H}^{\mathrm{div}}_0 \longrightarrow L^2$ is an extension of $\nabla\cdot : \boldsymbol{H}^1_0 \longrightarrow L^2$ in the sense that we have the remarkable property: $\widehat{\nabla}\cdot i = \nabla\cdot$ and $i^{\mathrm{t}}\,\widehat{\nabla} = \nabla$. This distinction between the two velocity spaces plays a key role in the convergence analysis of the fully discrete method as well as in its practical implementation.

The final velocity $\widehat{\boldsymbol{u}}^k$ is made to disappear from the fractional-step algorithm by substituting $\widehat{\boldsymbol{u}}^k = i\,\boldsymbol{u}^k - \Delta t\,\widehat{\nabla}(p^k - p^{k-1})$ into the equation of the viscous step, since we have

$$\begin{aligned} i^{\mathrm{t}}\,\widehat{\boldsymbol{u}}^k &= i^{\mathrm{t}}[i\,\boldsymbol{u}^k - \Delta t\,\widehat{\nabla}(p^k - p^{k-1})] \\ &= i^{\mathrm{t}}\,i\,\boldsymbol{u}^k - \Delta t\,i^{\mathrm{t}}[\widehat{\nabla}(p^k - p^{k-1})] \\ &= \boldsymbol{u}^k - \Delta t\,\nabla(p^k - p^{k-1}), \end{aligned}$$

where we used the property $i^{\mathrm{t}}\,\widehat{\nabla} = \nabla$. Then, the viscous step becomes:

$$\begin{cases} \dfrac{\boldsymbol{u}^{k+1}-\boldsymbol{u}^{k}}{\Delta t} - \nu\nabla^2\boldsymbol{u}^{k+1} + (\boldsymbol{u}^{k}\cdot\nabla)\boldsymbol{u}^{k+1} + \frac{1}{2}(\nabla\cdot\boldsymbol{u}^{k})\boldsymbol{u}^{k+1} \\ \qquad\qquad = \boldsymbol{f}^{k+1} - \nabla(2p^{k}-p^{k-1}), \\ \boldsymbol{u}^{k+1}{}_{|\partial\Omega} = \boldsymbol{b}^{k+1}. \end{cases} \tag{2.4}$$

By applying $\widehat{\nabla}\cdot$ to (2.3), we obtain the following Poisson equation:

$$\begin{cases} -\widehat{\nabla}^2(p^{k+1}-p^{k}) = -(\Delta t)^{-1}\,\nabla\cdot\boldsymbol{u}^{k+1}, \\ \dfrac{\partial(p^{k+1}-p^{k})}{\partial n}{}_{|\partial\Omega} = 0, \end{cases} \tag{2.5}$$

where we have used $\widehat{\nabla}\cdot i = \nabla\cdot$.

3 Second-order projection method

It is shown in Guermond and Quartapelle (1997) and proved in Guermond (1997) that the splitting error induced by this fractional step technique is of $\mathcal{O}((\Delta t)^2)$; as a result, second order order accuracy in time is possible if the time derivative in the momentum equation is replaced by a second order finite difference and the projection step is modified accordingly.

Following Guermond (1997), a three-level BDF is described hereafter, where the unconditional stability in the nonlinear regime is maintained by evaluating the skew-symmetric advection term semi-implicitly by means of a linear extrapolation in time of the advection velocity: $\boldsymbol{u}_\star^{k+1} = 2\boldsymbol{u}^{k} - \boldsymbol{u}^{k-1}$. The viscous step of the scheme reads

$$\begin{cases} \dfrac{3\boldsymbol{u}^{k+1} - 4i^{\mathrm{t}}\widehat{\boldsymbol{u}}^{k} + i^{\mathrm{t}}\widehat{\boldsymbol{u}}^{k-1}}{2\Delta t} - \nu\nabla^2\boldsymbol{u}^{k+1} + (\boldsymbol{u}_\star^{k+1}\cdot\nabla)\boldsymbol{u}^{k+1} \\ \qquad\qquad + \frac{1}{2}(\nabla\cdot\boldsymbol{u}_\star^{k+1})\boldsymbol{u}^{k+1} = \boldsymbol{f}^{k+1} - \nabla p^{k}, \\ \boldsymbol{u}^{k+1}{}_{|\partial\Omega} = \boldsymbol{b}^{k+1}, \end{cases} \tag{3.1}$$

and the projection step is performed as follows:

$$\begin{cases} \dfrac{3\widehat{\boldsymbol{u}}^{k+1} - 3i\,\boldsymbol{u}^{k+1}}{2\Delta t} + \widehat{\nabla}(p^{k+1}-p^{k}) = 0, \\ \widehat{\nabla}\cdot\widehat{\boldsymbol{u}}^{k+1} = 0, \\ \boldsymbol{n}\cdot\widehat{\boldsymbol{u}}^{k+1}{}_{|\partial\Omega} = \boldsymbol{n}\cdot\boldsymbol{b}^{k+1}. \end{cases} \tag{3.2}$$

Once the velocities $\widehat{\boldsymbol{u}}^{k}$ and $\widehat{\boldsymbol{u}}^{k-1}$ are eliminated by using (3.2), the two steps take the following form in practice:

$$\begin{cases} \dfrac{3\boldsymbol{u}^{k+1} - 4\boldsymbol{u}^{k} + \boldsymbol{u}^{k-1}}{2\Delta t} - \nu\nabla^2\boldsymbol{u}^{k+1} + (\boldsymbol{u}_\star^{k+1}\cdot\nabla)\boldsymbol{u}^{k+1} + \frac{1}{2}(\nabla\cdot\boldsymbol{u}_\star^{k+1})\boldsymbol{u}^{k+1} \\ \qquad\qquad = \boldsymbol{f}^{k+1} - \frac{1}{3}\nabla(7p^{k} - 5p^{k-1} + p^{k-2}), \\ \boldsymbol{u}^{k+1}{}_{|\partial\Omega} = \boldsymbol{b}^{k+1}; \end{cases} \tag{3.3}$$

$$\begin{cases} -\widehat{\nabla}^2(p^{k+1}-p^{k}) = -\dfrac{3}{2\Delta t}\,\nabla\cdot\boldsymbol{u}^{k+1}, \\ \dfrac{\partial(p^{k+1}-p^{k})}{\partial n}{}_{|\partial\Omega} = 0. \end{cases} \tag{3.4}$$

4 Space discretization and error estimates

For the spatial approximation of the viscous step, we introduce a finite element approximation $\boldsymbol{X}_{0,h} \subset \boldsymbol{H}_0^1$ for the intermediate velocity $\boldsymbol{u}_h$ and $N_h \subset H^1$ for the pressure p_h. Let the polynomial order of interpolation for the velocity be denoted by ℓ (≥ 1) and that for the pressure by ℓ', with $\max(\ell-1,1) \leq \ell' \leq \ell$. The two spaces $\boldsymbol{X}_{0,h}$ and N_h are assumed to satisfy the LBB condition (Ladyzhenskaya, Babŭska, and Brezzi).

The weak formulation of the advection–diffusion step (2.4) reads: For $k \geq 0$, find $\boldsymbol{u}_h^{k+1} \in \boldsymbol{X}_{b^{k+1},h}$ such that, for all $\boldsymbol{v}_h \in \boldsymbol{X}_{0,h}$,

$$\left(\frac{3\boldsymbol{u}_h^{k+1} - 4\boldsymbol{u}_h^k + \boldsymbol{u}_h^{k-1}}{2\Delta t}, \boldsymbol{v}_h\right) + \nu\,(\nabla \boldsymbol{u}_h^{k+1}, \nabla \boldsymbol{v}_h) + ((\boldsymbol{u}_{\star,h}^{k+1}\cdot\nabla)\boldsymbol{u}_h^{k+1}, \boldsymbol{v}_h) \quad (4.1)$$

$$+ \tfrac{1}{2}(\nabla\cdot \boldsymbol{u}_{\star,h}^{k+1}, \boldsymbol{u}_h^{k+1}\cdot \boldsymbol{v}_h) = (\boldsymbol{f}^{k+1}, \boldsymbol{v}_h) - \frac{1}{3}(\nabla(7p_h^k - 5p_h^{k-1} + p_h^{k-2}), \boldsymbol{v}_h).$$

The projection step has a unique expression only once the functional space for the end-of-step velocity is chosen. Many options are possible Guermond (1994), Guermond (1997); one of the simplest consists in selecting $\widehat{\boldsymbol{u}}_h^{k+1}$ in $\boldsymbol{X}_h + \nabla N_h$. Given this particular choice, it can be proven that the operator $\widehat{\nabla}_h$, the discrete counterpart of $\widehat{\nabla}$, coincides exactly with the restriction to N_h of the gradient operator; as a result, the projection step takes the following form: For $k \geq 0$, find $(p_h^{k+1} - p_h^k) \in N_h$ such that, for all $q_h \in N_h$,

$$(\nabla(p_h^{k+1} - p_h^k), \nabla q_h) = -3/(2\Delta t)\,(\nabla\cdot \boldsymbol{u}_h^{k+1}, q_h). \quad (4.2)$$

The description of the BDF projection method is concluded by recalling the following result established in Guermond (1997).

Theorem 1 *Under convenient regularity assumptions on the data* $\boldsymbol{f}$, $\boldsymbol{u}_0$, $\boldsymbol{b}$, *and provided the inf-sup condition is satisfied, the solution to the second order BDF projection scheme (4.1)-(4.2) satisfies the error bounds:*

$$\left\|\boldsymbol{u}_h^k - \boldsymbol{u}(t^k)\right\|_{\ell^2(\mathbf{L}^2(\Omega))} + \left\|\widehat{\boldsymbol{u}}_h^k - \boldsymbol{u}(t^k)\right\|_{\ell^2(\mathbf{L}^2(\Omega))} \leq c[\boldsymbol{u}, p](\Delta t^2 + h^{\ell+1}), \quad (4.3)$$

5 Numerical results and conclusions

The present method has been implemented using mixed P_1-P_2 finite elements.

The $\mathcal{O}((\Delta t)^2)$ accuracy of the BDF scheme has been tested with the following analytical solution in the unit square $[0,1]^2$: $u_x = -\cos x \sin y \sin(2t)$, $u_y = \sin x \cos y \sin(2t)$ and $p = -\frac{1}{4}[\cos(2x) + \cos(2y)]\,[\sin(2t)]^2$, for Reynolds number $Re = 100$, on a mesh of 2×40^2 P_1-P_2 triangles. Figure 1 shows the maximum value in time, over $0 \leq t \leq 1.5$, of the error in the L^2 norm for the pressure and the error in the H^1 and L^2 norms for the velocity. The saturation of the error as $\Delta t \to 0$ is due to the spatial discretization error, which is of order h^2 for the velocity (resp. pressure) in the H^1 (resp. L^2) norm, while it is of order h^3 for the velocity in the L^2 norm.

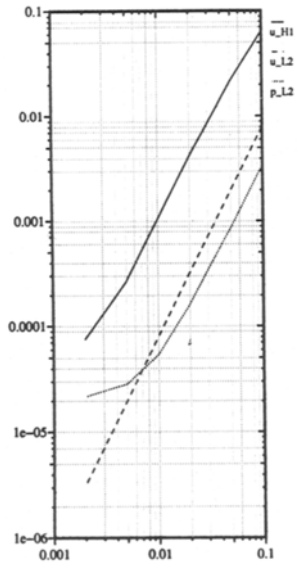

Fig. 1. Convergence tests in time for the BDF projection method, with P_1-P_2 FE. 2D analytical test problem for $Re = 100$.

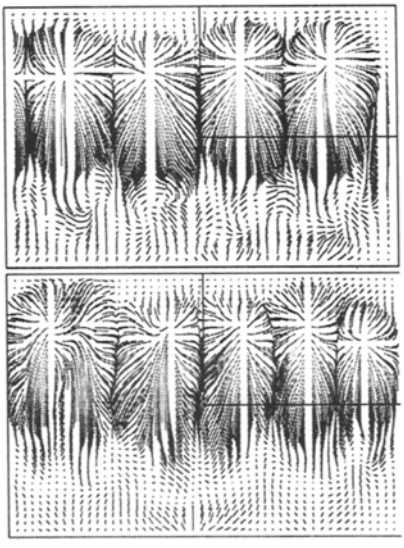

Fig. 2. 3D driven cavity problem with AR=1/1/3, for $Re = 3200$. Solution at times (left) $t = 50$ and (right) $t = 100$. Integral curves of the velocity field projected onto the plane $y = -0.49$.

The capability of the BDF-$(\Delta t)^2$ projection method to solve large-scale 3D problems has been assessed on the 3D driven cavity: $(|x| \leq 0.5) \times (|y| \leq 0.5) \times (|z| \leq 1.5)$, using a nonuniform mesh of $5 \times 20^2 \times 29$ P_1-P_2 tetrahedra for the half cavity (87579 P_2 nodes). The symmetry with respect to the plane $z = 0$ is assumed. First, the unsteady solution for $Re = 1000$ at $t = 6.25$ has been compared with its 2D counterpart in Figure 3. The secondary eddy located in the lower half of the downstream wall in the symmetry plane is found slightly weaker in the 3D simulation than in the 2D one as a consequence of the finite length of the cavity. This eddy vanishes at $1.25 \leq z \leq 1.3$.

In Figures 2 and 4 we show the integral curves of velocity field for $Re = 3200$ in some representative planes at times $t = 50$ and $t = 100$. No steady solution exists, and the number of Görtler vortices varies in time in accordance with other numerical solutions reported in Deville et al. (1992).

References

CHORIN, A J, *Math. Comp.*, **22**, (1968), 745–762 and **23**, (1969), 341–353.

DEVILLE, M, LÊ, T H AND MORCHOISNE, Y, EDS., *Notes on Numerical Fluid Mechanics*, **36**, Vieweg, Wiesbaden, (1992).

GODA, K, *J. Comput. Phys.*, **30**, (1979), 76–95.

GUERMOND, J-L, *C. R. Acad. Sc. Paris*, Série I, **319**, (1994), 887–892.

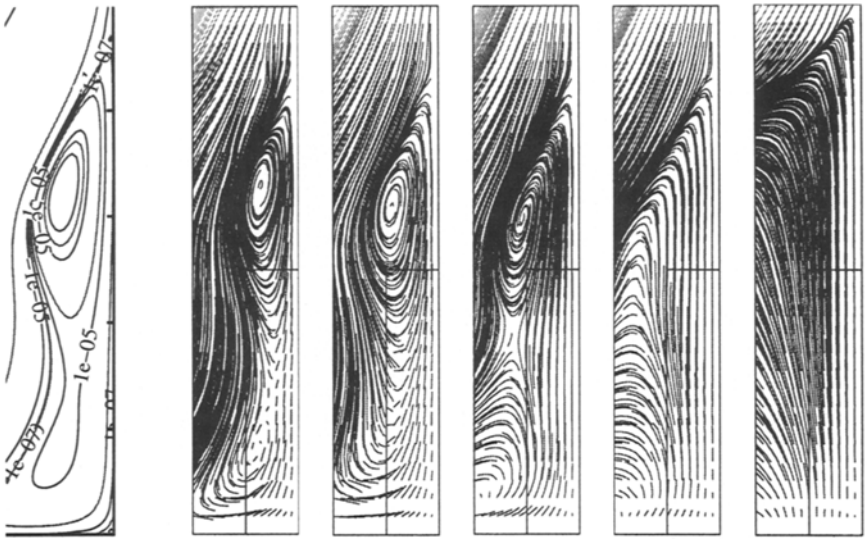

Fig. 3. 3D driven cavity problem with AR=1/1/3, for $Re = 1000$. Secondary eddy on the downstream wall at $t = 6.25$ in region: $0.4 \leq x \leq 0.5$, $-0.5 \leq y \leq 0$. Comparison of the 2D streamlines (left) with the integral lines of the 3D velocity field projected onto planes $z = 0$, 1, 1.25, 1.30, and 1.4 (from left to right).

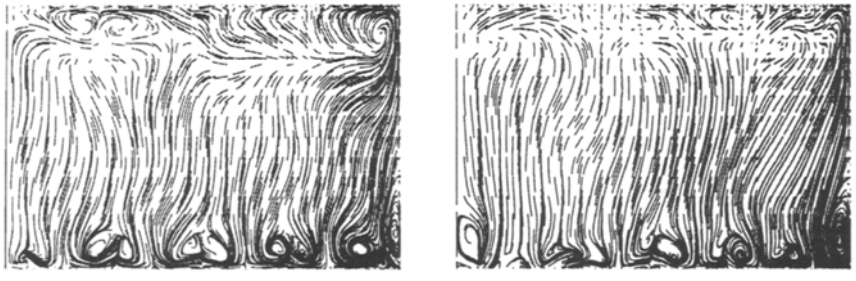

Fig. 4. 3D driven cavity problem with AR=1/1/3, for $Re = 3200$. Solution at times (left) $t = 50$ and (right) $t = 100$. Integral curves of the velocity field projected onto the planes $x = 0.13$ and $x = 0.18$.

GUERMOND, J-L, to appear in *Modél. Math. Anal. Numér.* (M^2AN), (1998) and *C. R. Acad. Sci. Paris*, Série I, **325** (1997) 1329–1332.
GUERMOND, J-L AND QUARTAPELLE, L, *J. Comput. Phys.*, **132**, (1997), 12–33.
GUERMOND, J-L AND QUARTAPELLE, L, to appear in *Numer. Math.*, (1998).
RANNACHER, R, *Lect. Notes Math.*, **1530**, Springer, Berlin, (1992), 167–183.
TEMAM, R, *Bull. Soc. Math. France*, **98**, (1968), 115–152.